6-2015

Investigation of Boat Hull Performance with Superhydrophobic Coating

Nolan Sayre
Union College - Schenectady, NY

Investigation of Boat Hull Performance with Superhydrophobic Coating

Nolan Sayre

Ann M. Anderson, Advisor

MER 498

Fall 2014/ Winter 2015

Union College, Department of Mechanical Engineering

Abstract

Aerogels are a nano-porous material that have the ability to be made chemically superhydrophobic. A durable boat hull coating of superhydrophobic aerogels could form the boundary conditions necessary to reduce drag in water and in turn improve overall boat performance. This project investigated whether a superhydrophobic aerogel coating could effectively reduce skin friction drag on a boat. Various techniques for superhydrophobic surface fabrication were researched and tested with the goal of maximizing the surface water contact angle. It was concluded that Nafion solution is not an effective material to adhere aerogels to a surface. Hydrophobic and non-hydrophobic aerogels were adhered to 3D printed boat hulls using double sided sticky tape. The hulls were attached to the bottom of a programmable boat and put through a series of performance tests with both hulls attached that were evaluated using video tracking software. It was found that average velocities of both the hydrophobic and non-hydrophobic aerogel boat hulls were higher than the average velocities of the control boat hulls. The average velocity of the hydrophobic boat hull was found to be significantly less than that of the non-hydrophobic boat hull. This surprising result may be due to the lack of surface air bubbles, characteristic of superhydrophobic surfaces, on the hydrophobic hull. Because of this possibility of an imperfect hydrophobic hull surface, it is still believed that superhydrophobic aerogels have the potential to reduce drag.

Table of Contents

Introduction

The goal of this project was to investigate the effect of hydrophobic boat hull coatings on the overall boat performance. Specifically, the focus was on creating a superhydrophobic surface using aerogels that could be applied directly to a boat hull and reduce friction drag. In order to fabricate this drag reducing surface, extensive research was conducted on superhydrophobic surfaces, drag reduction, and aerogel material.

Drag Reduction:

Friction exits in fluids in the form of drag. Drag force is the net force exerted by a fluid on a body in the direction of flow due to the combined effects of wall shear and pressure forces (Cengel 2006). The drag force can be split up into two components, pressure drag and skin friction drag. Pressure drag is also called form drag because it depends strongly on the shape of the solid body, specifically its frontal area. In flows at high Reynolds numbers the drag force comes mostly from pressure drag. This would occur in fluids with high velocities or low viscosity. An example of pressure drag dominance is a truck driving on the highway. The fluid, air, has low viscosity and the relative velocity of the fluid past the truck is high. On the other hand, friction drag dominates in flows at lower Reynolds numbers. Friction drag is the part of drag that is due directly to wall shear stress and is caused by frictional effects (Cengel 2006). Friction drag is proportional to surface area so the effects of friction drag are greater on bodies with larger surface area. Friction drag dominates in fluids with high viscosities, such as water. For example a fish would experience more friction drag than pressure drag. Figure 1 below shows the orientation of the drag force on a swimming fish.

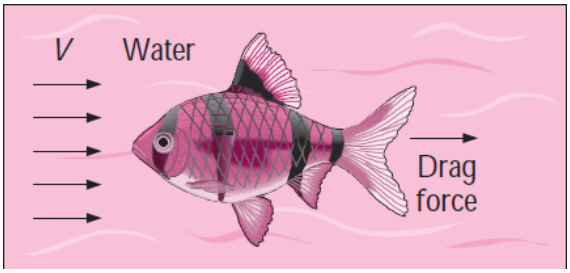

Figure 1: The orientation of drag force on a solid body moving through a fluid (Cengal 2006)

Drag reduction can occur from minimizing both pressure drag and friction drag, however the focus of this project was on the reduction of friction drag. Friction drag reduction has been researched extensively as a method to improve efficiency of vehicles from submarines to commercial airplanes. One of the most effective friction drag reduction mechanisms was developed by NASA and 3M Company to improve airplane fuel efficiency. Riblets are V-shaped angled grooves aligned in the direction of flow no deeper than a scratch (Dunbar 2004). This concept was originally modeled after shark skin, which contain riblet-like projections called dermal denticles allowing sharks to swim extremely fast. A comparison of riblet skin developed by 3M and shark skin is shown below if Figure 2.

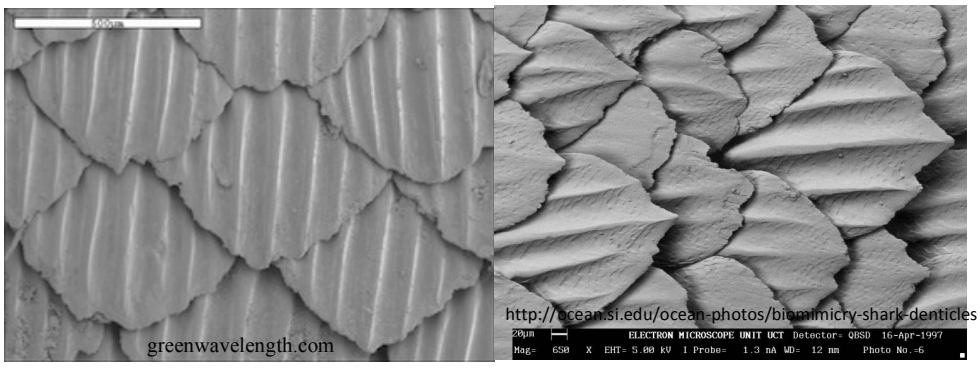

Figure 2: Riblet surface developed by 3M Company (Left), and shark skin (Right)

Riblets reduce drag in turbulent flows by disrupting the transverse motion of the fluid at the surface. The textured riblet surface exists in the Wenzel state meaning that there is full wetting

of the surface, compared to the Cassie-Baxter state where only partial wetting occurs. Not only have riblets been proven to save commercial airlines hundreds of millions of dollars annually, but they also have shown drag reducing effects in water (Dunbar 2004). The 1987 Americas Cup boat *Stars and Stripes* won a gold medal with a riblet coated hull allowing it to cut through the water with ease (Dunbar 2004). Although riblets have proven effective, an alternative method of drag reduction is through the use of superhydrophobic surfaces.

Hydrophobic Surfaces:

Hydrophobic surfaces were first inspired by the unique characteristics of the lotus leaf which allow it to repel water. Materials such as the lotus leaf cause water to bead off rather than wetting the surface and sticking. Although to the naked eye the lotus leaf looks normal, it actually has micro and nano-scale structures on its surface as well as a hydrophobic chemical composition. Hydrophobic materials have become an increasingly researched topic in recent years because of their application in self-cleaning, anti-fouling, and drag reduction. Hydrophobicity is most commonly quantified by measuring the contact angle, the angle between the plane of the surface and the tangent to the surface of a droplet of water resting on it (Barabasz 2011). Hydrophobic surfaces are classified as surfaces exhibiting contact angles between 90° and 140°, while superhydrophobic materials have contact angles between 140° and 180°. Figure 3 below shows how the contact angle (θ) is measured.

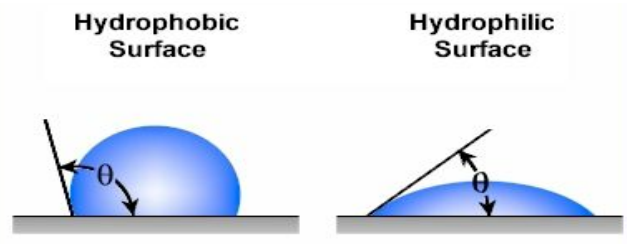

http://awesci.com/super-hydrophobic-surfaces-unbelievable/

Figure 3: Comparison between hydrophobic and hydrophilic contact angles

Contact angles can be estimated using the Young-Laplace equation which describes the surface tension between the water droplet and the surrounding air. The contact angle estimation takes into account the radius, height, and general shape of the water drop (Young-Laplace Equation). The equation for the contact angle, θ_c, is shown below.

$$\theta_c = \arccos\left(\frac{r_A cos\theta_A + r_R cos\theta_R}{r_A + r_R}\right)$$

Where θ_A is the advancing contact angle, θ_R is the receding contact angle, r_A is the advancing radius, and r_R is the receding radius.

Hydrophobic surfaces that result from low surface free-energy are most commonly called chemically hydrophobic surfaces. When a surface is sufficiently different chemically from water, significant intermolecular reactions do not occur between the surface and water. This lack of interaction causes water to be repelled from the surface (Rodriguez 2014). Many hydrophobic materials have been developed and are available at the consumer level. Rust-Oleum NeverWet and Ultratech Ultra-Ever Dry are two hydrophobic surface coatings that have applications in anti-wetting, anti-icing, anti-corrosion, and self-cleaning (Never-Wet). Ultra-Ever Dry claims to produce contact angles greater than 170°, which is almost perfectly hydrophobic.

Superhydrophobic surfaces can result from a combination of chemical hydrophobicity and micro-scale surface roughness. When submerged in water, superhydrophobic surfaces can entrap air between microstructures, creating a surface with both air-water and solid-water interfaces (Samaha 2012). Figure 4 below depicts a superhydrophobic surface submerged in water.

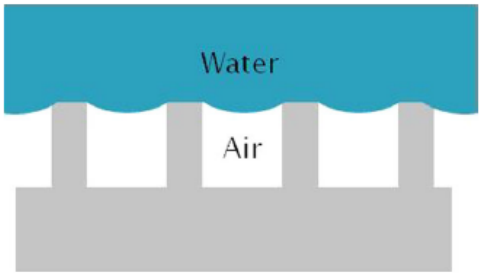

Figure 4: Superhydrophobic surface submerged in water (Nilsson 2010)

Superhydrophobic surfaces are fabricated by either creating hierarchical structures on hydrophobic substrates, or by chemically modifying hierarchical structured surfaces to have low surface free-energy. Methods of superhydrophobic surface fabrication include phase separation, electrochemical deposition, sol-gel processing, and wet chemical reactions (Guo 2011). In a study by Rothstein et al superhydrophobic surfaces exhibiting a contact angle of 151° were fabricated by sanding a Teflon surface (Nilsson 2010). Superhydrophobic surfaces have also been developed by etching micro-scale features into a hydrophobic surface. However, this method is extremely expensive due to the precision manufacturing required to form microfeatures (Nilsson 2010). It is the morphological hydrophobicity of superhydrophobic surfaces that creates the potential for drag reduction.

Drag Reduction on Superhydrophobic Surfaces:

The no-slip condition of fluid mechanics states that a fluid in direct contact with a solid "sticks" to the surface due to viscous effects. Therefore, the fluid layer adjacent to the solid surface has no relative velocity with respect to the surface. The no-slip condition is responsible for the development of the boundary layer next to the surface where viscous effects are significant (Cengel 2006). The viscous effects of the fluid are directly related to the force of

friction drag. Since the no-slip condition applies everywhere along the surface, the larger the surface area is, the larger the friction drag force is.

As previously stated, superhydrophobic surfaces form a combination of air-water and solid-water interfaces when submerged in water (Samaha 2012). It is the presence of this air-water interface that leads to drag reducing abilities. The trapped air is supported by the surface tension of water and the chemical hydrophobicity of the surface. Therefore, only the very tips of the microfeatures contact the liquid, and a reduced shear air-water interface exists everywhere else over which water slips (Rothstein 2009). This reduces the total area of the solid-liquid interface, decreasing the effects of the no-slip condition and in turn decreasing friction drag. When the surface is viewed macroscopically, the overall boundary condition no longer exists as no-slip, but rather as partial-slip. This phenomenon is called the Cassie-Baxter model which describes the partial wetting of surfaces due to both solid-liquid and air-liquid interfaces. Figure 5 shows the difference between fluid flow over a normal surface and a superhydrophobic surface existing in the Cassie state.

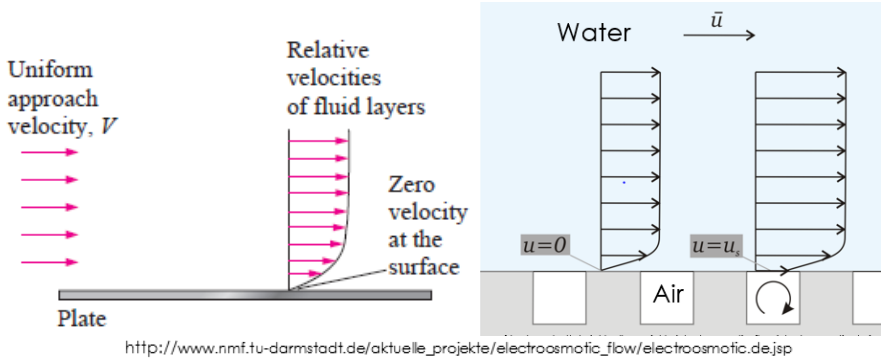

Figure 5: No-slip condition on flat plate (Left), partial-slip on superhydophobic surface (Right)

Superhydrophobic Aerogels:

Silica aerogels are porous ceramic materials consisting of 90-99% air by volume. Aerogels have high surface area, low density, low thermal and electrical conductivity, and are visibly transparent. This unique combination of properties makes them suitable for a variety of applications from thermal and acoustic insulation, to chemical sensors. Aerogels are fabricated through a basic two-step procedure. A wet gel is formed through a sol-gel polymerization reaction of precursor chemicals, then the sol-gel solvent is extracted leaving behind a dry, rigid nanostructure. Although aerogels are typically hydrophilic, they can be made chemically to be hydrophobic. Hydrophobic aerogels are formed by organically modifying the silica gels to have a mixture of TMOS (tetramethoxysilane) and MTMS (methyltrimethoxysilane) (Anderson, Hydrophobic 2009). The combination of chemical hydrophobicity with the nanoporous structure allows aerogels to be made into a superhydrophobic material. Although other superhydrophobic materials exist, aerogels are of interest because of their ability to be manufactured quickly and easily. The technique of rapid supercritical extraction developed by Gauthier et al. allows aerogels to be fabricated in under three hours, for approximately seven times cheaper than other methods (Gauthier 2004).

Previous Work at Union College:

The drag reduction properties of hydrophobic aerogels have been studied in various previous experiments. In a 2014 study using an aerogel coated rotational viscometer, the aerogel coating was shown to reduce drag by 20-30% in laminar flow (Rodriguez 2014). For her 2010 senior thesis at Union College, Sarah Schinasi developed a superhydrophobic aerogel surface to be used as a coating for crew racing shells (Schinasi 2010). Similarly, Robin Barabasz studied the effect of a superhydrophobic aerogel coating on hydrodynamic drag (Barabasz 2011). As a result of high uncertainty in data, neither of these studies were conclusive.

In his 2013-2014 senior project, *Hull Design of a Radio-Controlled Boat Using 3D Printing*, Dylan Magida investigated the performance of different boat designs, specifically looking at three major hull types; displacement, semi-displacement, and planing (Magida 2014). Magida used CAD modeling to make a computer model of each type of hull and utilized high-resolution 3D printing to fabricate accurate prototypes. After being attached to a radio-controlled boat, the boat hulls were put through a series of performance tests and video tracking software was used to track the motion of the boat (Magida 2014). For my project I will be building on Magida's work by using his most versatile boat hull, the V-bottom semi-displacement to conduct my drag reduction tests. I will utilize Magida's experimental setup including the remote controlled boat, video camera and tracking software, and planing ability test to measure the drag reducing abilities of a superhydrophobic boat hull coating.

Project Goal:

The goal of this project was test the effect of a hydrophobic aerogel coating on an autonomous boat. The content of the remainder of this paper includes a description of fabrication methods for multiple aerogel surfaces as well as a detailed description of the technique used to measure the hydrophobicity of the surfaces. Additionally, the test methods and boat performance results are explained to determine whether the aerogels impacted boat performance.

Preparation of Hydrophobic Surfaces

Aerogel surfaces were fabricated using aerogel solutions as well as applying aerogels directly to an adhesive. The quality of each surface was determined by its hydrophobicity. The goal of the surface preparation was to maximize the hydrophobicity of the aerogel surface prior to testing. When this was accomplished, the aerogels were applied to the bottom of the plastic boat hull shells for testing.

Measuring Hydrophobicity:

The hydrophobicity of aerogel powders as well as aerogel-Nafion films was measured using a Kruss Drop Shape Analyzer (DSA 100) located in the Union College Aerogel Lab. This instrument, pictured below in Figure 6, places a water droplet of specific volume onto a surface using a precision needle.

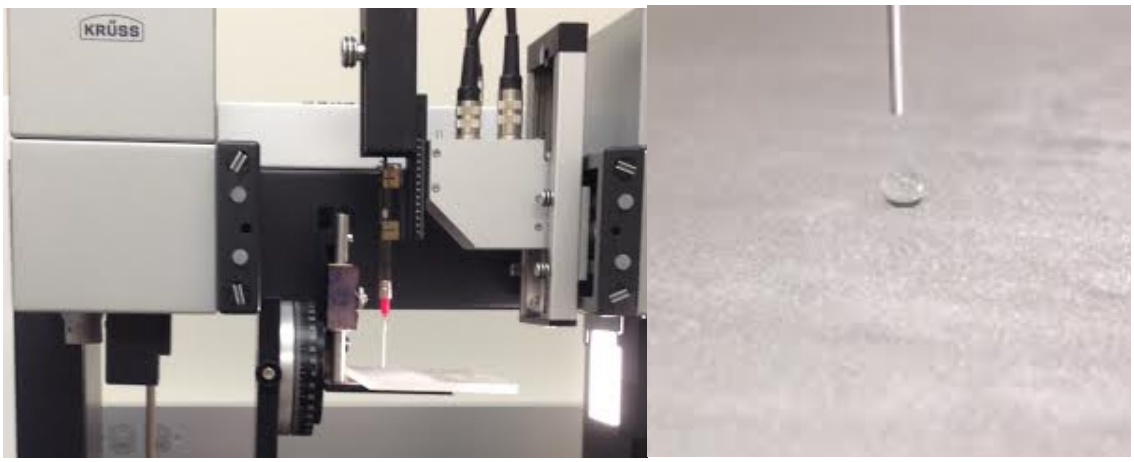

Figure 6: Kruss Drop Shape Analyzer used for contact angle measurements

A high definition camera produces an image of the water drop that is imported into the computer program DSA3. This program uses the Young-Laplace sessile drop fitting to estimate the contact angle of the drop. Figure 7 shows the DSA3 program fitting a drop and measuring the tangent contact angle.

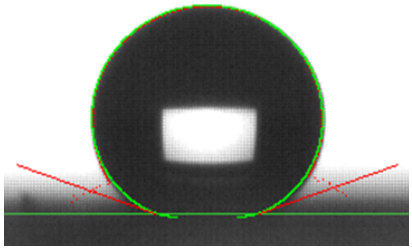

Figure 7: DSA3 contact angle measurement calculation, contact angle =160.7°

It is important to note that DSA3 can misinterpret the water drop shape and make an inaccurate contact angle estimation. Particularly, the program wrongly identifies the outline of the water drop, which distorts the contact angle calculation. This error is shown below in two water drops with the same volume and very similar shape. The contact angle for the drop on the left was calculated to be 153°, and 119° for the drop on the right.

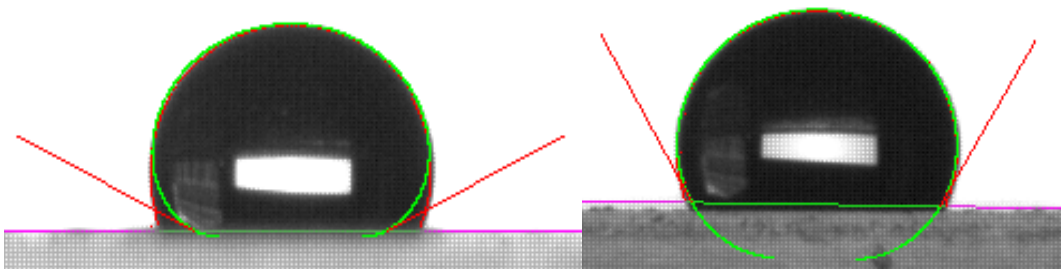

Figure 8: Poorly calculated contact angle (Left), accurate contact angle (Right)

Because of this variability, it was important to visually check the water drop outline produced by DSA3 to ensure accurate contact angle calculations.

In order to become familiar with the Kruss Drop Shape Analyzer and DSA3 program twenty contact angle measurements were taken on an aerogel-Nafion surface made by Schinasi (Schinasi 2010). Her double sided coating of aerogels on a piece of Plexiglas produced an average contact angle of 155±7°.

Aerogel-Nafion Surface:

Extensive testing was conducted on making solutions consisting of aerogel, Nafion, and propanol. Previous research had shown that hydrophobic aerogel surfaces could be fabricated using this technique. The focus of this research was spent optimizing the ratio of the three ingredients to make a functional solution.

Past work by Sarah Schinasi and Robin Barabasz

In order to fabricate superhydrophobic surfaces, a solution comprised of crushed aerogel powder, a solution of Nafion, water, and propanol, and additional propanol was used. Nafion is a synthetic polymer that was tested by Schinasi to be an effective solvent for an aerogel solution (Schinasi 2010). It acted as a binding agent while allowing the aerogels to retain their superhydrophobic characteristics. Schinasi's research determined that the most hydrophobic solutions were formed with the ratio 250% aerogel by weight to Nafion. This ratio was also confirmed by Barabasz who replicated Schinasi's final aerogel film, recording an average contact angle of 161°. Barabasz determined that the most successful Nafion solution was 5 wt. % polymer content, 15-20 wt. % water, and 75 wt. % alcohol (propanol) (Barabasz 2011). She also determined that the most successful superhydrophobic films were fabricated using superhydrophobic aerogels that were not pre-gelled during the fabrication process. These aerogels exhibited significantly higher hydrophobicity than aerogels that had been pre-gelled.

Based on this research, aerogel-Nafion solutions for this project were made with about 250% aerogel by weight to Nafion, using the Nafion solution 5 wt. % polymer content, 15-20 wt. % water.

Preliminary aerogel-Nafion films

Initial aerogel-Nafion films were fabricated using RB7 aerogels made by Robin Barabasz and Nafion solution left over from Barabasz's project. These aerogels were made using 15.93 mL MTMS, 15.93mL TMOS, 103.125 mL Methanol, 13.5mL water, and 0.507mL Ammonia. The hot press program 2B was used which had no pre-gel (Barabasz 2011). RB7 aerogels were crushed for 15 minutes using a mortar and pestle. Prior to the testing of aerogel-Nafion solutions, tests were conducted to ensure the hydrophobicity of the aerogels being used. The crushed RB7 aerogels were sprinkled onto a microscope slide covered in double sided sticky tape, creating a layer of aerogels on the slide. The aerogels were spread uniformly over the tape and extra aerogels not sufficiently stuck down were brushed off. Ten contact angle measurements were taken and the average contact angle was found to be $143 \pm 7°$, proving that the aerogels were superhydrophobic.

Initial aerogel-Nafion recipes were based off of the most effective ratios of aerogel to Nafion found by Schinasi and Barabasz. The first solution was made by scaling up Schinasi's best recipe (0.0244g aerogel, 0.156mL Nafion) 15x. This included 0.366g aerogel, 2.50mL Nafion, and 0.313mL propanol. The volume of propanol was scaled down to be ¼ times Schinasi's final recipe which included 1.25mL propanol. When mixed together, the aerogels stayed as a powder and visually it was clear that not enough solvent was present. The extremely

low density of aerogels was considered as one reason for the lack of solvent in the scaled recipe. When the mass of aerogels was increased with the same scale as the volume of Nafion or propanol, the volume of aerogels increased much faster than that of liquids. In order to eliminate potential errors due to scaling, the next solution was made using Barabasz's exact final recipe which included 0.218g aerogel, 2mL Nafion, and 4mL propanol. This solution was mixed together for five minutes in a small beaker using a metal spatula. It formed a solution of low viscosity that was able to be painted onto a microscope slide. This slide was left in the hood to dry for 24 hours. When the slide dried contact angle measurements were taken and it was found that the average contact angle was $103 \pm 38°$. This low contact angle sparked another examination of the fabrication in search of possible errors. It was hypothesized that one reason for the low contact angles exhibited by the early aerogel films was the Nafion solution being used. The Nafion solution was about three years old, which may have caused some of its properties to be comprised due to water and propanol evaporation. Therefore, when SRG money became available, 50mL of new Nafion was purchased with the same ratios suggested by Barabasz (5 wt. % polymer content, 15-20 wt. % water, and 75 wt. % alcohol).

Aerogel-Nafion Films from Fresh Nafion

50mL of new Nafion was purchased with the same ratios suggested by Barabasz (5 wt. % polymer content, 15-20 wt. % water, and 75 wt. % alcohol). In order to ensure the quality of the secondary aerogel-Nafion films, a new batch of RB7 aerogels was crushed into a powder using mortar and pestle. The aerogels were crushed dry for 30 minutes. It was desired to determine the optimal ratios of aerogel powder to Nafion solution to propanol. Therefore, ten aerogel-Nafion slides were fabricated with varying amounts of aerogel, Nafion, and propanol. Table 1 shows the resulting contact angles of the ten aerogel-Nafion films.

Table 1: Aerogel-Nafion films made with new Nafion and crushed RB7 aerogel

Slide #	Coating	aerogel (g)	Nafion (mL)		Propanol (mL)		CA
1	Single	0.109	1	(9.2)	0.4	(3.7)	**n/a**
2	Single	0.109	1	(9.2)	0.4	(3.7)	**n/a**
3	Single	0.0244	0.156	(6.4)	0	(8.2)	**128±20**
4	Single	0.025	0.25	(10)	0	(0)	**119±16**
5	Double	0.05	0.35	(7)	0.2	(4)	**98±16**
6a	Single	0.218	2	(9.2)	4	(18.3)	**119±10**
6b	Single	0.218	2	(9.2)	4	(18.3)	**115±16**
6c	Single	0.218	2	(9.2)	4	(18.3)	**124±5**
6d	Double	0.218	2	(9.2)	4	(18.3)	**117±12**
6e	Poured	0.218	2	(9.2)	4	(18.3)	**n/a**

This tables displays the coating style (single coat, double coat, or poured on), amount of aerogels, Nafion, and propanol, and the average contact angle of the slide. The numbers in parentheses represent the ratio of Nafion or propanol to aerogel for that solution in (mL/g). This table shows that the maximum average contact angle was found on Slide #3 with CA=128°±20°. While a contact angle of 128° defined the surface as hydrophobic, the high standard deviation was reason for concern. All average contact angles were based on ten to twenty contact angle measurements taken at random locations on the aerogel-Nafion surface using 2μL water drops. In many of the slides contact angles between 140°-155° were measured, yet on the same slides contact angles less than 100° were also measured. This high deviation in results shows that the aerogel-Nafion solution was not drying uniformly on the surface of the slide. The least

hydrophobic films were found to be Slide #1, 2, and 6e. These slides were so hydrophilic that contact angle measurements could not be taken on them. When these slides were dried it was observed that large concentrations of aerogels were resting on the surface of the slides. When the surface was touched, these aerogels sprinkled off, leaving a highly uniform surface. This problem seemed to occur in Slides #1 and #2 due to the high concentration of aerogels in relation to propanol. Although in Slide #6e the concentration of aerogels to propanol was much less, the solution was poured onto the slide. This application technique seemed to inhibit all of the aerogels from adhering to the surface, leaving free aerogels resting on the surface. After reviewing this data as well as work down by Schinasi and Barabasz, it appeared that the most effective aerogel-Nafion surfaces were single or double coated. It was also clear that higher concentrations of aerogels do not necessarily lead to increased contact angle.

With these results in mind, a third set of aerogel-Nafion films were fabricated (Slides #7 a, b, c, d, e). These films were made using Barabasz's final recipe with ½ of the propanol, making the solution 0.218g aerogel, 2mL Nafion, and 2mL propanol. RB7 aerogels were used that were crushed using propanol by Barabasz and dried in a petri dish. The appropriate quantities of aerogel, Nafion, and propanol were combined in a glass vial and the solution was mixed using a sonic mixing machine for 8.5 minutes. After the solution was inspected visually to ensure that the aerogels had dissolved, the half inch paint brush was used to paint a single coat of the solution onto four microscope slides. These slides were left to dry in the hood for 24 hours. Table 2 below shows the resulting contact angles of the slides measured using the Kruss Drop Shape Analyzer.

Table 2: Contact angle measurements of aerogel-Nafion solution #7

	CA [°]	Std Dev [°]

Slide #7a	113	9
Slide #7b	113	8
Slide #7c	n/a	n/a
Slide #7d	118	17
Slide #7e	106	5

Slides #7a, #7b, and #7e proved to be the most consistent slides made yet. Although the contact angles were still lower than desired, the slides did not exhibit any hydrophilic spots. Visually the #7 slides looked like the most consistent coating yet. Slide #7e is shown below in Figure 9

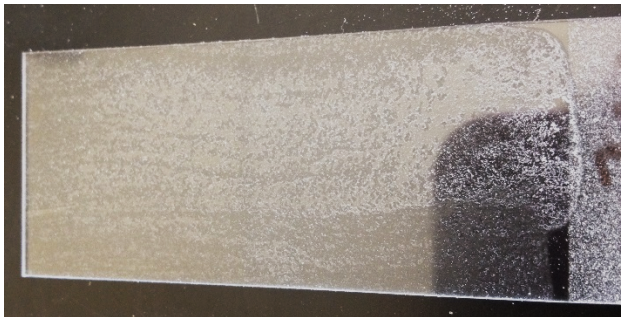

Figure 9: Microscope slide coated with aerogel-Nafion solution #7

Slide #7c was used as a test for the durability of the aerogel-Nafion coating. A drop of water was placed on the surface of the slide and was rubbed around to see how well the coating would stay in place. Unfortunately, the aerogel-Nafion coating rubbed off quite easily, leaving a hydrophilic surface. Slide #7d produced contact angles very similar to slides #7a and #7b, however in a few spots the 2mL water drop would not stick to the surface, indicating superhydrophobicity. When a drop size of 4mL was used, the drop stuck to the surface and contact angles of 147° and 150° were measured. This was the first time that superhydrophobic regions were found on a slide that didn't also have hydrophilic regions.

Aerogel-Nafion Coating on 3D Printer Material

Aerogel-Nafion were next tested on 3D printer plastic to determine if the glass surface material could have had a negative effect on the aerogel-Nafion solution. By using the plastic rather than the glass for testing, the contact angle results would correlate directly to how the solution would react on the actual boat hull shell. The flat bottom boat hull shell made by Dylan Magida in 2014 was available and therefore was cut up into pieces roughly 2" by ¾". The grey 60 Stratasys 3D printer material that was used to manufacture this hull was the same material that the new boat hull shell would be printed using.

The first series of aerogel-Nafion surfaces on the plastic were made holding the mass of aerogel and volume of propanol constant, while varying the volume of Nafion in the solution. This solution was painted onto the plastic using a ½" paint brush to apply a single coat of solution. Table 1 below shows the corresponding average contact angles calculated from ten random contact angle measurements taken on each surface.

Table 3: Table of contact angles for series of solutions on 3D print plastic

0.1g aerogel, 1mL propanol	
0.5mL Nafion	CA=126±7°
1mL Nafion-A	CA=117±6°
1mL Nafion-B	CA=122±6°
1.5mL Nafion-A	CA=115±5°
1.5mL Nafion-B	CA=114±8°

These results show that the 0.5mL Nafion solution produced the highest contact angle of 126±7°. As the volume of Nafion in the solution increased, the contact angle decreased. However, there was not a significant difference in hydrophobicity between any of the test pieces, with only a 12° difference between the smallest and largest contact angles. Although none of the pieces were superhydrophobic, the results were promising in other ways. The standard

deviations on all of the pieces were below 10°, making the surfaces the most consistent that had been made thus far. Visually, there was not a considerable difference between any of the pieces. Images of the aerogel-Nafion surfaces are shown below in Figure 10.

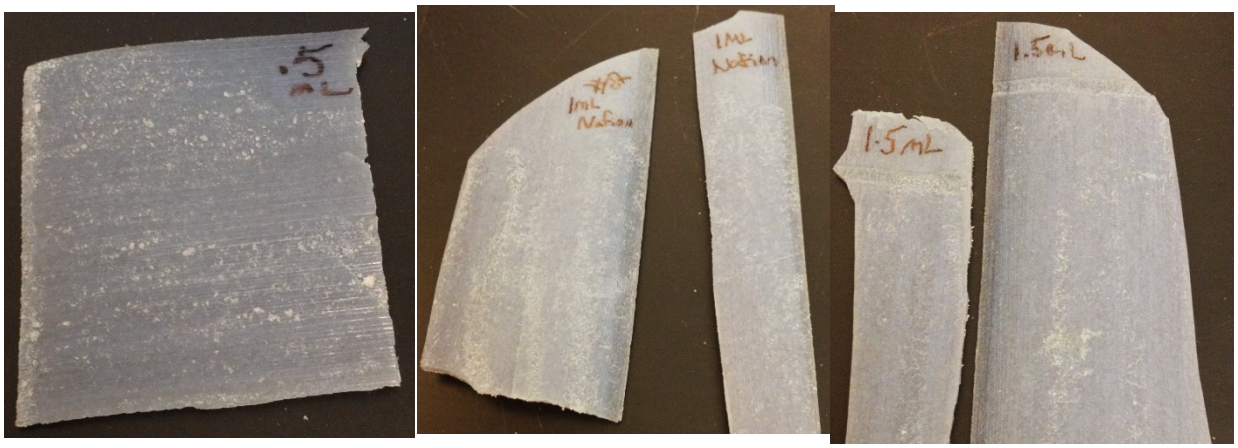

Figure 10: From left to right, the 0.5mL Nafion, 1mL Nafion, and 1.5 mL Nafion test pieces

On all five plastic pieces, clumps of aerogel can be seen on the surface that formed while the solution was drying. It appears that the 0.5mL Nafion piece has the most defined clumps of aerogels out of the five pieces. Slightly less aerogel can be seen on the surfaces of the 1.5mL Nafion pieces, however the distribution of aerogel visually looks similar on all samples. It is important to note that this was the first set of aerogel-Nafion surfaces made where there were no hydrophilic spots found on any of the pieces. There were also multiple spots found on the 0.5mL Nafion piece that were too hydrophobic for the 2µL drop to stick to the surface.

As previously stated, it was observed that the aerogel powder had formed some clumps on the surface of the plastic while it was drying, specifically on the 0.5mL Nafion piece. After all of the initial contact angles were measured, this excess aerogel was rubbed off of the 0.5mL piece by gently rubbing a finger over the surface. The piece was rubbed such that all of the loose aerogel fell off, leaving only the aerogel powder that was adhered to the surface of the plastic.

After this was done, ten more contact angle measurements were taken at random spots on the surface. The average contact angle was found to be 135±9°, showing a 9° increase after the excess aerogel was rubbed off. It was hypothesized that this was because the aerogels that were stuck well to the surface were the finest particles and formed a more uniform and therefore more hydrophobic surface than the larger particles that easily rubbed off.

After this set of tests, a new set of hydrophobic aerogels were received from Nate Hawthorne to replenish the stock of aerogel powder. The aerogels were PTES/TEOS made in June, 2014. These aerogels were crushed for twenty minutes using a mortar and pestle into a very fine powder. Using double sided sticky tape on a glass microscope slide, these aerogels produced an average contact angle of 155±9°, confirming that they were superhydrophobic. Unless stated otherwise, all aerogel surfaces fabricated after this point used these aerogels.

The next surface that was fabricated served to determine whether the most hydrophobic solution from the previous set (0.1g aerogel, 1mL propanol, 0.5mL Nafion) could be made more hydrophobic by increasing the amount of aerogel in the solution. In order to test this, a solution was made with 0.15g aerogel. However, with this amount of aerogel, the volume of propanol had to be increased to 2.5mL in order to liquefy the solution. This surface was put under the same test as the previous piece by rubbing off all of the excess aerogel powder resting on the surface. Then, both pieces were placed in a beaker of water for twenty hours. After sufficient drying time, the contact angles were measured again. The results of the tests are shown below.

Table 4: Contact angle results from three tests, original, after rubbing, and after soaking

	Ratio to aerogel	Original	After Rubbing	After Soaking
0.15g aerogel, 0.5mL Nafion, 2.5mL Propanol	1-3.3-16.7	129±12°	137±5°	77±4°
0.1g aerogel, 0.5mL Nafion, 1mL	1-5-10	126±7°	135±9°	103±5°

Propanol				

These results show that adding more aerogel to the solution did not successfully increase the contact angle of the surface. While both the "original" and "after rubbing" contact angles were a few degrees higher for the larger mass of aerogel, the results were within the standard deviation of both contact angles. Similar to the 0.1g aerogel surface, the contact angle increased after the excess aerogel was rubbed off of the surface. For the 0.15g aerogel piece, the contact angle increased by 8° while the standard deviation decreased by 7°. However, the most significant outcome of these tests was seen in the "after soaking" results. The contact angle of the 0.1g aerogel surface decreased by 32°, making the surface barely hydrophobic. The contact angle of the 0.1g aerogel surface decreased by 60°, putting the contact angle below 90° making it no longer hydrophobic.

These results were very significant because the application of hydrophobic surfaces is naturally when they are exposed to water. The fact that the hydrophobic characteristics of the surfaces deteriorated after exposure to water implies that this method of superhydrophobic aerogel surface fabrication is not the best option. This is true particularly for this project where the aerogel surface will be subjected to a medium velocity flow of water while attached to the boat hull during testing. Although Nafion has proven to be a good adhesive for making aerogel surfaces in past research, these results show that Nafion may not the ideal material for the process. Because of this, the decision was made to halt further testing of aerogel-Nafion surfaces for the purpose of this project.

Alternate Hydrophobic Surfaces:

The understanding of superhydrophobicity from a combination of chemical and morphological hydrophobicity led to an interesting question; can microridges with the potential to be made superhydrophobic be fabricated using 3D printing? The conditions necessary for morphological hydrophobicity require microfeatures less than 60μm apart. The Stratasys Objet500 Connex 3D printer at Union College claimed to have the capabilities to print at a resolution of 15 μm. The capabilities of manufacturing a microridged plastic piece using 3D printing that could be made superhydrophobic were explored as another potential way to create a drag reducing surface. A full description of this process can be found in Appendix B.

An alternative method of fabricating aerogel surfaces that was explored was using a spray on adhesive that could be sprayed directly onto the boat hull shells. Aerogels would then be pressed against the surface leaving an exterior coating of aerogels. Two sprays made by The 3M Company were researched, 3M 77 Super Multipurpose Adhesive Aerosol and 3M Marine Grade Spray Adhesive. Both of these sprays were of interest because of their fast acting bond and multipurpose application. However, it was decided that a more durable alternative to spray on adhesives would be using high strength double sided sticky tape. Sheets of double sided sticky tape were purchased that would be cut to fit the contours of the boat hull. From using double sided sticky tape to test the hydrophobicity of previous aerogel powders, it was known that it could be used to make superhydrophobic surfaces.

Double Sided Sticky Tape Surface:

In order to apply the aerogels to the surface of the boat hull, first the double sided sticky tape sheets were cut into four rectangles to cover the four distinct surfaces on the boat hull shell. One side of the tape was peeled away as each sheet was pressed onto the bottom of the boat hull. Then a scalpel was used to carefully cut the tape along the edge of each face, leaving the four

pieces fit exactly to the boat. Images of the sticky tape being applied to the hull and the finished surface prior to the application of aerogels are shown below in Figure 11.

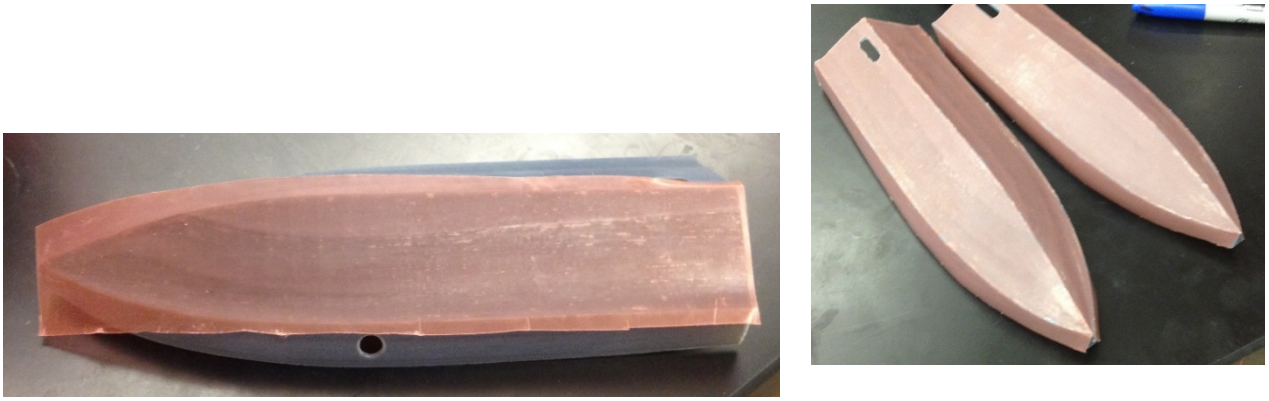

Figure 11: Application of sticky tape sheets to the 3D printed boat hull shells

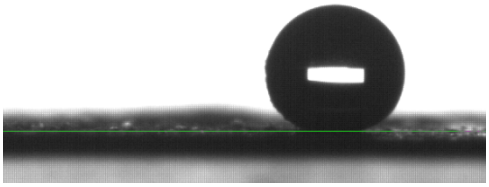

The aerogels that were used for the surfaces were superhydrophobic TMOS aerogels and non-hydrophobic aerogels. The recipe for the non-hydrophobic aerogels included TMOS (23 mL), Methanol (75 mL), DI Water (10 mL) and 1.5 M Ammonia (0.74 mL). The recipe for the hydrophobic aerogels included TMOS (5mL), MTMS (5mL), MeOH (31.1mL), DI Water (4.08mL), and 1.5 M NH_4OH (0.154mL). This mixture was sonicated for five minutes. Both batches of aerogels were crushed in a plastic container using a pestle for twenty minutes. Initial contact angles were measured for both the hydrophobic and non-hydrophobic aerogels. The aerogels were coated onto the double sided sticky tape which was stuck to microscope slides. Twenty contact angles were taken at ten random spots on the slides using 4µL water drops. The non-hydrophobic aerogel surface produced a contact angle of 80±11°, proving that it was

hydrophilic. The hydrophobic aerogel surface was so hydrophobic that most 4μL drops would not stick to the surface. However, a maximum contact angle of 168° was measured on a water drop, showing superhydrophobicity. An image of this water drop is shown below in Figure 12.

Figure 12: Water drop on hydrophobic aerogels attached to double sided sticky tape

After the pink top sheet on the sticky tape was removed, the aerogels were applied the surface by sprinkling aerogel powder over the bottom of the hull and then pressing and spreading the powder into the surface. This was done continuously for approximately 10 minutes. Unfortunately the boat hulls would not fit in the viewing area of the Kruss Drop Shape Analyzer so contact angle measurements on each surface could not be measured. In order to get a visual reference for the quality of each surface, water drops were put on the bottom of both hulls, shown below in Figure 13.

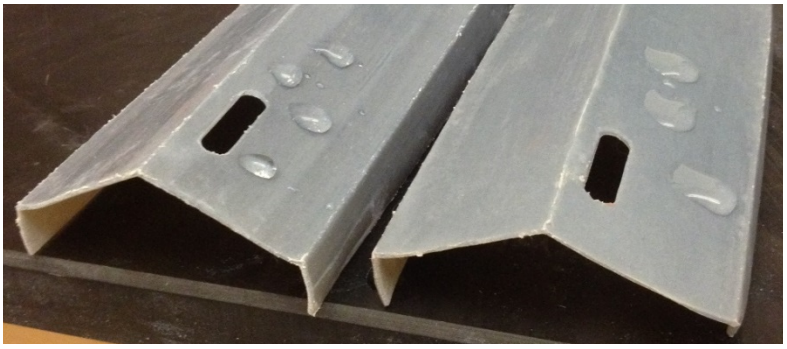

Figure 13: Water drops on the hydrophobic hull (Left) and non-hydrophobic hull (right)

It can be seen that the water drops stuck significantly more to the non-hydrophobic hull than the hydrophobic hull. The left image shows that the water drops bubbled on the surface of the hydrophobic hull indicating that a hydrophobic surface was created.

As a result of the aerogel surface fabrication portion of this project a few noteworthy points were determined. Although Nafion had been used in past experiments to make hydrophobic aerogel surfaces, the adhesive was not the ideal bonding agent for aerogels. Double sided sticky tape created aerogel surfaces sufficient for the purpose of this project, however future research should explore alternative methods of creating an aerogel surface that can be painted on. This characteristic of the aerogel-Nafion surfaces allowed for a wide range of applications. A repeatable method for creating hydrophobic aerogel surfaces that could be painted onto surfaces would allow the application of aerogels to expand dramatically.

Boat Performance Test Procedure and Results

The boat performance tests were conducted using a small boat that was altered from remote controlled to autonomous. The boat motion was tracked using video tracking software and the average hull velocities were compared.

Boat Modifications:

The remote controlled boat used for this project was the same boat that Dylan Magida used for his 2014 senior project. Because of this, the boat had already seen sufficient use and wear when it was received for this project. In early testing of the boat's functionality, it was noted that when controlled by the remote control, the boat could only run at full power for a few seconds before the motor would shut off. After this point, the batteries were too drained for the receiver on the boat to pick up the signal from the remote control. After testing the remote control on land and in water it was decided that for the purpose of this project, the lack of reliability in the remote controlling device could have serious effects on the boat's performance and in turn the testing results. To alleviate this potential problem the remote controlling device was removed from the boat and was replaced by a programmable microcontroller. The A-Star 32U4 Microcontroller was purchased from Polulu.com and installed into the boat. This microcontroller allowed a specific power to be programmed into the boat, removing the variability in boat power from the remote controller. Arduino was used to program the power delivered to the motor and the time the motor would run for. The Arduino programming allowed the power to be specified as a value between 0 and 255, with 255 being the maximum power setting. Additionally, a new boat battery was purchased for testing since it was discovered that two of the battery packs had lost significant power storage from overuse. During testing, the red

battery refers to the new battery and the black battery refers to the existing battery. These were the only two batteries used in testing.

The boat hull design for this project was also based off of the hull design created by Dylan Magida. Magida's 3D boat hull models were created using Union College's Faro Arm to accurately model the remote control boat hull shape. SolidWorks was used to create the boat hull shells with appropriate geometries corresponding to the remote control boat. Magida's V-bottom boat hull shell was chosen as the test hull for this project because, since the remote control boat has a V-bottom, this hull fit the remote control boat most accurately. Modifications were made to the boat hull shell in order to reduce water intake between the boat and the boat hull shell. However, due to 3D printing limitations it was decided to conduct the testing using Magida's original boat hull shell design. A detailed description of the proposed improvements to the boat hull shell can be found in Appendix A.

Testing and Analysis Methods:

A series of six trials were performed using each of the boat hulls. Three out of the six trials used the red battery and three trials used the black battery. These trials were conducted consecutively starting with the battery at full charge. NH_B_1 refers to the first trial of the non-hydrophobic hull using the black battery, when the battery was fully charged. NH_B_2 refers to the second trial using the black battery. This trial was conducted directly after the first trial with the black battery without restoring the battery to full charge. This testing method was used due to the extended amount of time it took to restore the batteries to full charge even after running for only five seconds. However, using this test method each trial for the hydrophobic hull corresponds to a trial for the non-hydrophobic hull with equal battery charge.

Similar to the initial tests, these performance tests were conducted in the Union College swimming pool. The boat was run at the edge of the pool, between the metal siding and the first floating lane marker. This provided roughly an eight inch lane for the boat to drive in. This was important because, since the manual steering was removed along with the remote control device, the lane ensured that the boat moved in a relatively straight line. At the beginning of each trial, the battery was connected to the boat and the boat was placed in the center of the testing lane pointing straight forward. The boat was programmed to have a fifteen second delay to the start of the motor after connecting the battery allowing the boat to stabilize in the water before accelerating forward. At the end of each trial the battery was disconnected so that the motor only pulled power from the battery for exactly five seconds during each trial. The Arduino code used for the boat trials can be found in Appendix C.

The trials were filmed and video tracking software was utilized to analyze the motion of the boat. The program Tracker provided displacement, velocity, and acceleration data for boat. Using this program, the boat's location was pin pointed at each frame of the video. After specifying a coordinate system and a scale, the boat's motion could be plotted against time. A screenshot of the program tracking the boat during one trial is shown below in Figure 14.

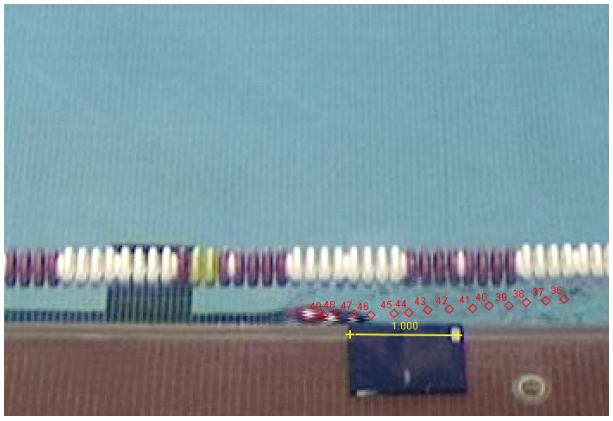

Figure 14: Tracker program mapping out the motion of the boat during a trial

The red diamonds show the previous marked points of the boat during the last fifteen frames. The yellow line is the measuring stick used as the length reference. The blue notebook shown had markings on it for one foot, therefore the program produced velocity measurements in feet per second. Not visible in the image is the coordinate axis that was defined prior to analysis. For all trials the origin was placed at the boat's starting point and the positive x-axis was aligned along the side of the pool. Therefore, the x-velocity and x-displacement was recorded during analysis.

Using the Tracker program, instantaneous velocity measurements for each time step were recorded and plotted against time. The instantaneous velocities for the six trails for each boat hull were averaged at each time step to generate the average instantaneous velocities for the hydrophobic and non-hydrophobic boat hulls.

Preliminary Testing:

During initial testing of the boat in the pool, both with and without the 3D printed hulls attached, the power and time settings for the boat were altered in order to determine the best combination. During the first test of the boat after the removal of the remote controller, the boat was set at max speed, power 255, for 10 seconds. However, the speed of the boat was highly underestimated and the boat easily made it across the pool and hit the opposing wall well before the motor turned off. Because of this the power was decreased to 128 for five seconds. When the boat was tested with the plastic boat hull shell attached, there was not enough power for the boat accelerate to planing speed. Before the baseline testing began the power was increased to 180 for seven seconds.

Before testing the aerogel surface, both 3D printed boat hull shells were tested to make sure that there was no significant bias in between the two hulls. Five trials were conducted, alternating the hulls that were used. After the second trial it was apparent that the power was still too low for the boat to reach planing speed and therefore the power was changed to the final setting of 220 for 5 seconds. The five trials were analyzed and the velocities were plotted which is shown below in Figure 15.

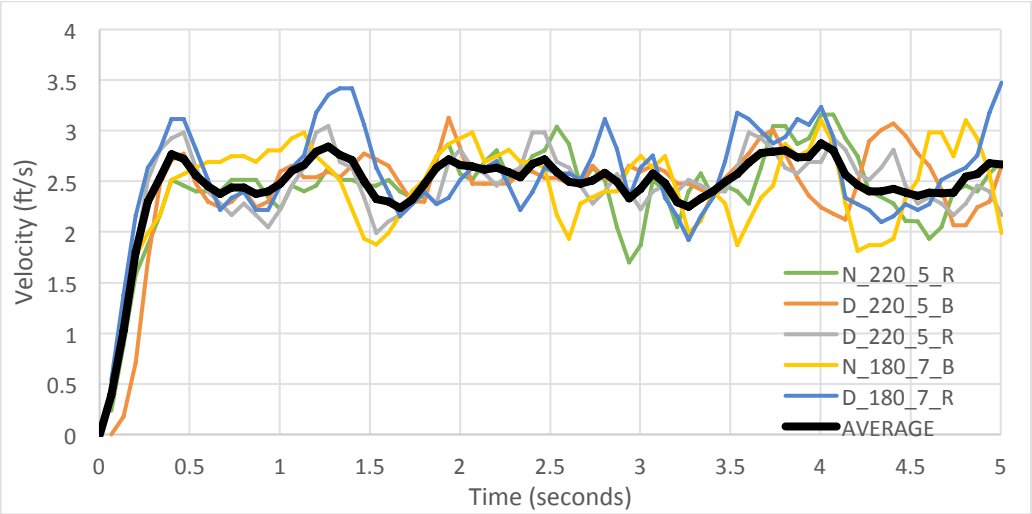

Figure 15: Velocity plots of the boat hull shells without aerogels

The legend shown depicts the boat hull (D-Dylan's or N-Nolan's), the power setting (180 or 220), the motor run time (5 or 7 seconds), and the battery used (R-red battery or B-black battery). This graph shows that the instantaneous velocities throughout the trials had little deviation between the two boat hulls. For every trial the velocity appeared to level out around 2.5 ft/s while jumping around above and below this value. It should be noted that although the velocity data looks very scattered rather than truly leveling out at a value, this is because the Tracker program is producing instantaneous velocities rather than time averaged velocities. Therefore, while tracking the boat using the program any small error in pinpointing the exact location can

result in what shows up on the graph as a large spike or dip in velocity. In reality, the velocity of the boat is far smoother and more uniform. This can be seen in the plots of boat displacement. Below in Figure 16 the displacement graph with a best fit line for trial N_220_5_R is shown.

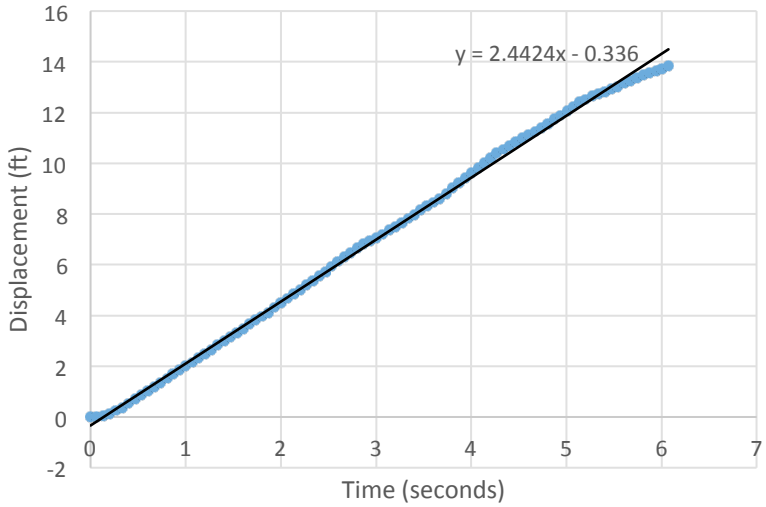

Figure 16: Plot of boat displacement for initial trial N_220_5_R

This graph shows that the displacement of the boat is increasing relatively linearly, indicating that the boat reached a constant velocity. In order to get a time averaged velocity, a linear fit was generated for the displacement plots of each trial. The fit line for N_220_5_R is shown in Figure 16 along with the equation corresponding with the line. Table 5 below shows the time averaged velocities calculated using this method for each trial. The average velocities were calculated using the displacement data from two seconds to five seconds in order to eliminate initial acceleration.

Table 5: Time averaged velocities for initial boat hull trials

Trial	Velocity (ft/s)
D_180_7	2.61
D_220_5_B90%	2.57
D_220_5_B70%	2.57
N_180_7	2.61
N_220_5_R100%	2.58
AVERAGE	**2.58±.04**

This table provides important information for two reasons. First, the average velocity of 2.58 ft/s for all the trials supports the velocity plots in Figure 15 that show the velocities leveling out around 2.5 ft/s. Secondly, the standard deviation of the average velocity, ±0.04 ft/s, is exceptionally small. This shows that significant differences do not exist between the two boat hulls. Because of this, the boat hull chosen for the hydrophobic and non-hydrophobic surfaces would not affect or compromise the results. This data allowed the boat hull bias to confidently be removed from the tests. This initial set of trials show that the average velocity of the boat with the 3D printed boat hull without aerogels is 2.58±.04 ft/s.

Testing Aerogel Boat Hull Coatings:

Instantaneous velocity data was recorded for the hydrophobic and non-hydrophobic boat hulls during identical tests as performed on the control trials. Figure 17 below shows the instantaneous velocity graph for the hydrophobic boat hull.

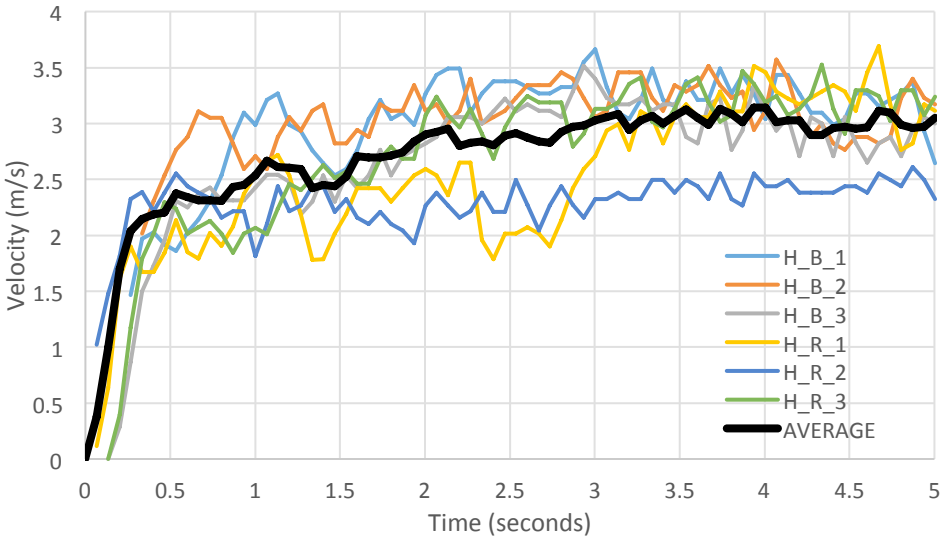

Figure 17: instantaneous velocity data for the hydrophobic boat hull

This graph shows that the hydrophobic boat hull reached a maximum velocity of about 3 ft/s. However, there is some considerable variation in the velocity results, specifically in the velocities of H_R_1 and H_R_2, which are noticeably lower than the rest of the trials. This result is of particular interest because of the experimental method. The batteries were run consecutively, so there was less battery power for H_R_3 than H_R_1 and H_R_2. However, the boat performed considerably better in H_R_3 than the other two trials using the red battery. Possible explanations for this variation will be addressed in a later section.

The non-hydrophobic hull was put through an identical series of tests and the instantaneous velocity results are shown below in Figure 18.

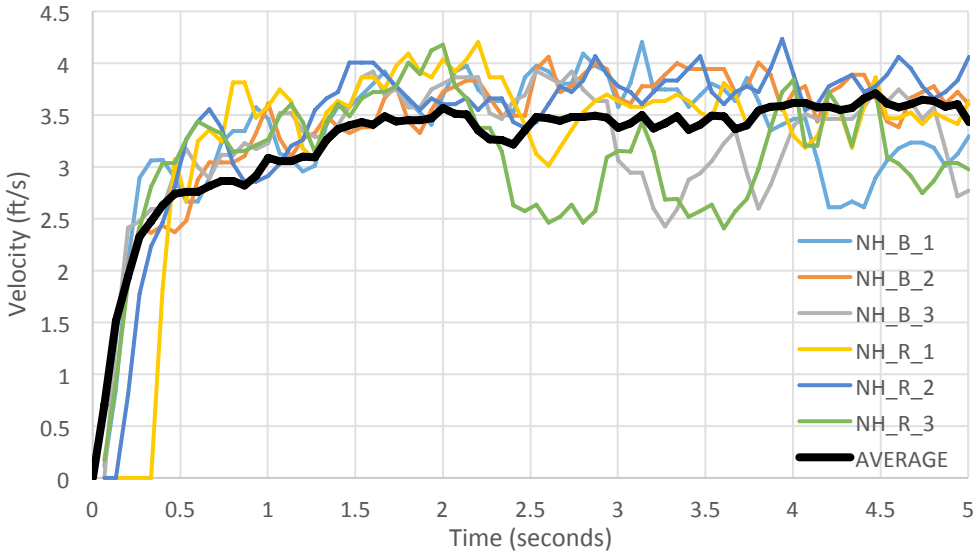

Figure 18: Instantaneous velocity data for the non-hydrophobic boat hull

This graph shows that the velocities of the non-hydrophobic hull leveled out around 3.5 ft/s. The time to accelerate to this speed was roughly two seconds. In general, the velocity graphs for each trial are very consistent, with the exception of NH_R_3 and NH_B_3 from two seconds to five seconds. These two plot lines show sharp dips in velocity during the last three seconds of the trials.

The average velocity lines for the hydrophobic and non-hydrophobic hulls were plotted together which is shown below in Figure 19.

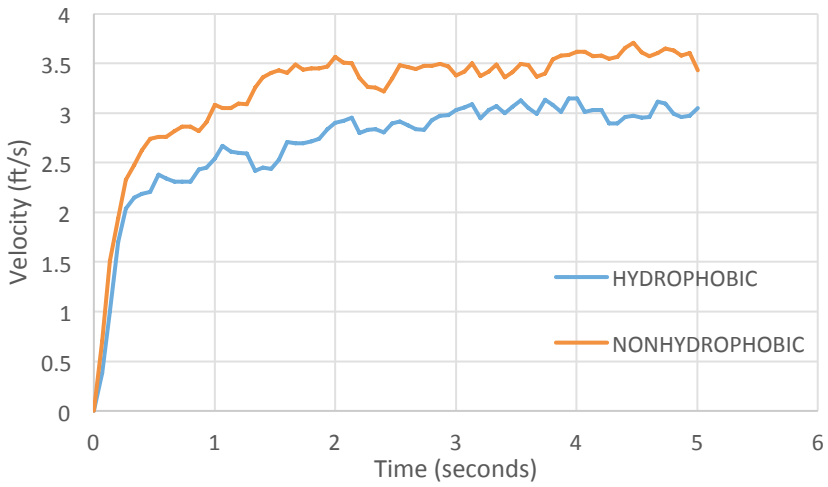

Figure 19: Comparison of hydrophobic and non-hydrophobic average velocities

This graph shows a distinct difference between the velocity of the hydrophobic and non-hydrophobic boat hulls. The non-hydrophobic boat hull reached a velocity of about 3.5 ft/s whereas the hydrophobic boat hull reaches a velocity of about 3 ft/s. This difference in velocities was measured again when the time averaged velocities were calculated for each hull. The time averaged velocities were calculated using the displacement graphs generated using Tracker. A linear line of best fit was generated using the data from two seconds to five seconds to produce an average terminal velocity for each trial. Table 6 below shows the average velocities for each trial of the hydrophobic boat hull.

Table 6: Time averaged velocities for the hydrophobic boat hull trials

Hydrophobic	
Trial	Velocity (ft/s)
H_R_1	2.90
H_R_2	2.38
H_R_3	3.17
H_B_1	3.28
H_B_2	3.22
H_B_3	3.07
AVERAGE	**3.00±0.33**

This table shows that the velocity averaged over all the trials was calculated to be 3.00±0.33 ft/s. The time averaged velocities for the non-hydrophobic boat hull are shown below in Table 7.

Table 7: Time averaged velocities for the non-hydrophobic boat hull

Non-hydrophobic	
Trial	Velocity (ft/s)
NH_B_1	3.55
NH_B_2	3.78
NH_B_3	3.53
NH_R_1	3.53
NH_R_2	3.78
NH_R_3	2.99
AVERAGE	**3.48±0.30**

This table shows that the average velocity of the non-hydrophobic boat hull was calculated to be 3.48±0.30 ft/s. This is significantly higher than the velocity of the hydrophobic boat hull being 3.00±0.33ft/s.

Discussion of Results

These results show that the non-hydrophobic boat hull achieved the highest velocities, averaging at 3.48±0.30 ft/s. This is considerably faster than the average velocity of the hydrophobic boat hull which averaged a velocity of 3.00±0.33 ft/s. Although these results do not agree with the hypothesized results, it may not mean that non-hydrophobic surfaces reduce drag more effectively than hydrophobic surfaces. It should be noted that when the hydrophobic boat hull was put in the water, no air bubbles were observed on the surface of the hull. This means that the surface may not have been as hydrophobic as anticipated. Although both the hydrophobic and non-hydrophobic aerogels were adhered to the sticky tape using similar methods for approximately ten minutes, the quality of the hydrophobic surface is unknown. Even after applying aerogels consistently, after ten minutes when the surface was touched some stickiness could still be felt on the surface. This means that the entire surface was not coated in aerogels. This stickiness was not felt on the non-hydrophobic surface, indicating that the non-hydrophobic aerogels may have bonded to the sticky tape better than the hydrophobic aerogels.

Additionally, there were multiple limitations in the experimental setup of this experiment that may have proved compromising to the results. First, due to the camera and space used for testing, there was limited room for the boat trials to be conducted. In order to use the video tracking software, the camera had to be stationary while the object being tracked moved through the frame. This limited the testing space to the size of the camera frame. With the camera as far from the pool as possible to maximize the frame size, the boat could only drive for about five seconds before leaving the view of the camera. While data was able to be gathered form this, ideally a longer test would have been conducted where the boat could drive for at least ten seconds. This would allow a definitive maximum velocity to be measured.

Another potential source of error was the lateral motion of the boat during the trials. Since the ability to manually steer the boat was removed along with the remote controller, the rudder angle was fixed during the trials. It was attempted prior to each trial to ensure that the rudder was aligned as straight as possible, however this was not always effective. During storage of the boat prior to this year, the rudder had received pressure that caused it to bend sideways slightly. Because of this the boat naturally wanted to turn right even when the rudder was straight. During some trials the boat would end up maneuvering in a somewhat zig-zag motion between the left and right barriers of the testing lane. Since the Tracker was only measuring motion in the forward direction, any lateral movement resulted in a loss of forward velocity. It is believed that this error could be attributed to some of the larger dips in velocity seen in Figure 99 and Figure 99, particularly in trials NH_R_3, NH_B_3, and H_R_1.

Conclusions

Although this experiment did not show the benefit of superhydrophobic aerogel surfaces, the results do show that aerogels are capable of drag reduction. The average velocities of both the hydrophobic and non-hydrophobic aerogel hulls were higher than the velocities of the boat hulls without any aerogels. Additionally, it was found that Nafion is not the most effective way to adhere aerogels to a surface. After extensive testing, consistent superhydrophobic aerogel-Nafion surfaces could not be fabricated in a repeatable process. Future research should explore alternative adhesive methods for creating aerogel surface. Similarly, future invesitigations of aerogels as a drag reduction mechanism should consider the use of water tunnels or other controlled apparatus. This would allow the boundary between the fluid and the surface to be viewed and analyzed.

Acknowledgements

I would like to thank the following people for their contributions toward the completion of this project: Union College Professors Ann Anderson, Mary Carroll, Bradford Bruno, and David Hodgson, Rhonda Becker, Stan Gorski, Kathy Ryan, Coach Scott Felix, Dylan Magida, Alex Cavert, Stephan Grant, and The Aerogel Team. This project would not be possible without the Student Research Grant funding.

References:

[1] Anderson, Ann M., Caleb W. Wattley, and Mary K. Carroll. "Silica Aerogels Prepared via Rapid Supercritical Extraction: Effect of Process Variables on Aerogel Properties." *Journal of Non-Crystalline Solids* 108th ser. 335.101 (2009).

[2] Anderson, Ann M., Mary K. Carroll, Emily C. Green, Jason T. Melville, and Michael S. Bono. "Hydrophobic Silica Aerogels Prepared via Rapid Supercritical Extraction." *J SOl-Gel Technol* (2009).

[3] Barabasz, Robin. *Effects of Superhydrophobic Aerogel Surface Coatings on Drag Reduction*. Thesis. Union College, 2011.

[4] Carroll, Mary K., and Ann M. Anderson. "Use of Rapid Supercritcal Extraction Method to Prepare Aerogels from Various Precursor Chemistries." *Polymer Preprints* 52(1).31 (2011).

[5] Cengel, Yunus A., and John M. Cimbala. Fluid Mechanics Fundamentals and Applications. New York: McGraw Hill, 2006.Print.

[6] Dunbar, Brian. "NASA RIBLETS FOR STARS & STRIPES." *NASA*. NASA, 21 Nov. 2004. Web. <http://www.nasa.gov/centers/langley/news/factsheets/Riblets.html>.

[7] Gauthier, Ben M., Et Al. "A Fast Supercritical Extraction Technique for Aerogel Fabrication." Journal of Non-Crystalline Solids 350 (n.d.): 238-43. Science Direct. Web. 6 Nov. 2004.

[8] Guo, Zhiguang. "Superhydrophobic Surfaces: From Natural to Miomimetic to Functional." *Journal of Colloid and Interface Science* 1st ser. 353.2 (2011): 335-55. Web.

[9] Magida, Dylan. *Hull Design of a Radio-Controlled Boat Using 3D Printing*. Thesis. Union College, 2014.

[10] "NeverWet." N.p., n.d. Web. 13 Nov. 2014. <http://www.neverwet.com/>.

[11] Nilsson, Michael A., Robert J. Daniello, and Jonathan P. Rothstein. "A Novel and Inexpensive Technique for Creating Superhydrophobic Surfaces Using Teflon and Sandpaper." *Journal of Physics D: Applied Physics* (2010).

[12] Rodriguez, Justin E., Ann M. Anderson, and Mary K. Carroll. "Hydrophobicity and Drag Reduction Properties of Surfaces Coated with Silica Aerogels and Xerogels." *Journal of Sol-Gel Science and Technology* (2014).

[13] Rothstein, Jonathan P. "Slip on Superhydrophobic Surfaces." *Annual Review of Fluid Mechanics* 109th ser. 42.89 (2009).

[14] Samaha, Mohamed. "Effects of Hydrostatic Pressure on the Drag Reduction of Submerged Aerogel-particle Coatings." *Colloids and Surfaces. A, Physiochemical and Engineering Aspects*(2012): Web.

[15] Schinasi, Sarah. *The Effects of Surface Finish on Drag: Coatings of Racing Shells*. Thesis. Union College, 2010.

[16] "Young–Laplace Equation." *Wikipedia*. N.p., 11 May 2014. Web.

Appendix A: Boat Hull Shell Modifications

After reviewing Magida's work as well as talking with him about his project, improvements to the hull design were decided upon. One problem with the boat hull shells attaching the remote control boat was that water was getting between the hull shell and the boat. Water appeared to be splashing over the stern end of the boat while the boat was transitioning into a planing mode. In order to mitigate this problem, Magida's design was modified to have splash guards along the upper rails extending along the length of the boat. A curved encasing was put over the tip of the bow to inhibit water from coming over the bow when the boat was moving at low speeds. Water was also coming between the boat hull shell and the boat through cutouts on the bottom and side of the boat hull shell where water intake and outtake holes were located. The water outtake cutout on the side of the boat was moved forward 0.15in in order to better line up with the outtake hole. The cutout on the bottom of the boat for the water intake was made significantly smaller to fit tightly around the water intake tube. Figure 19 below show the modified boat bull next to the original design.

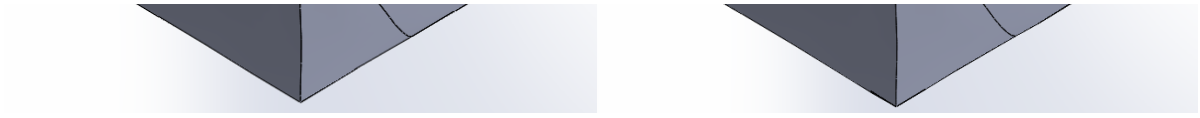

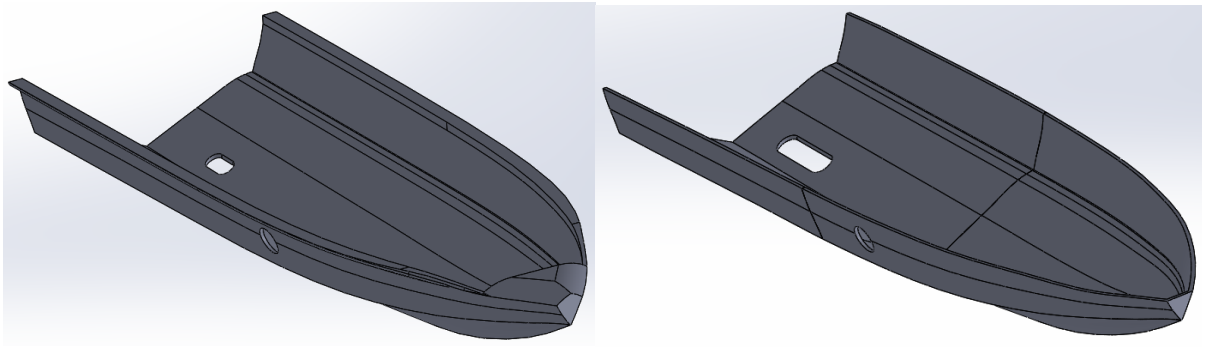

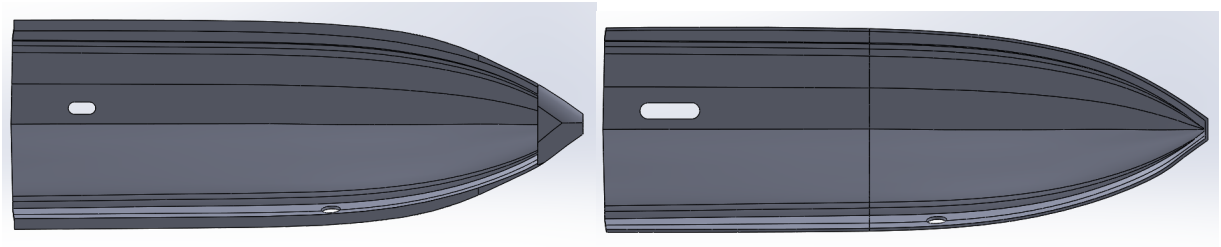

Figure 19: CAD model of modified boat hull design (Left), origninal boat hull design (Right)

The top images clearly show the encasing over the bow as well as the splash gaurds extending down the side of the hull. In the middle and bottom images the reduced size of the water intake cutout on the bottom of the hull can be seen.

Magida's boat hull shells were printed using the Union College Stratasys Objet500 Connex Milti-Material 3D Printer using the polypropylene material RGB8530DM (Grey 60). This material was chosen due to its water resistance, strength, and slight flexibility (Magida). No noticeable problems were discovered from using this material, so it was chosen as the 3D printing material for the new boat hulls.

Appendix B: 3D Printing Microridged Piece

A rectangular piece was designed in SolidWorks with 30μm by 30μm ridges cut into one half of the piece, shown below in Figure 20.

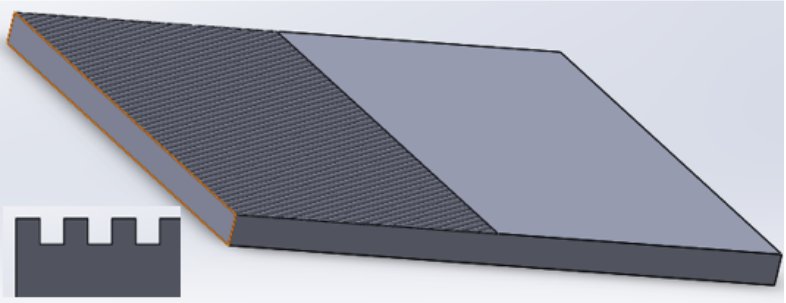

Figure 20: SolidWorks model of 30μm ridged test piece

This piece was printed using the Stratasys Connex 3D printer. Initial visual observations did now show any signs of the microridges, however that was to be expected because of their scale. One notable observation was that the fabrication method of the 3D printer left horizontal lines on the piece marking the path made by the nozzle. Unfortunately, this piece was unable to be examined under microscope due to technical malfunctions of the SEM.

While the SEM was being fixed, a second microridged piece was designed and printed. This piece had 60μm ridges along half of one side. On the top of the smooth side "Nolan" was cut out of the piece extruding in 100μm. This design was included with the hopes that if nothing else, that feature could be visible with the naked eye. Figure 21 below shows the printed 30μm test piece

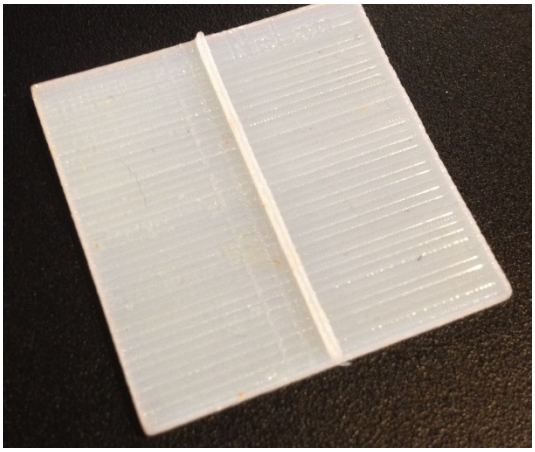

Figure 21: 3D printed piece with 30μm ridges on the left side.

This image clearly shows the incidental horizontal lines formed from the 3D printing process. These ridges can also be felt when a finger is rubbed across the surface. A few vertical lines can be seen just to the left of the separating barrier in the middle of the piece. These visible ridges provided hope for the presence of the 30μm microridges on the left side of the piece. Also in Figure 10 on the top right of the piece "Nolan" can faintly be seen written across the top. This was visible to the naked eye, proving that the printer was capable of printing depth resolution as small as 100μm, the depth of the letters.

Initially when the piece was removed from the printer, filler material was surrounding the piece in a very thin layer. In order to remove this excess material, the piece was put into a sealed tank where a pressure washer sprayed off the filler material. However, even after pressure washing there was still evidence of the filler material on the surface of the piece. Because morphological hydrophobicity requires clear unfilled voids between microfeatures, it was decided to take extra steps to ensure the removal of all filler material. The 3D printed piece was submerged in a beaker of Sodium Hydroxide, which dissolved all of the remaining filler material. After this process the piece looked visually more clean and precise.

With the help of Alex Cavert the 60μm microridged piece was examined using the SEM. The images produced are shown below in Figure 22.

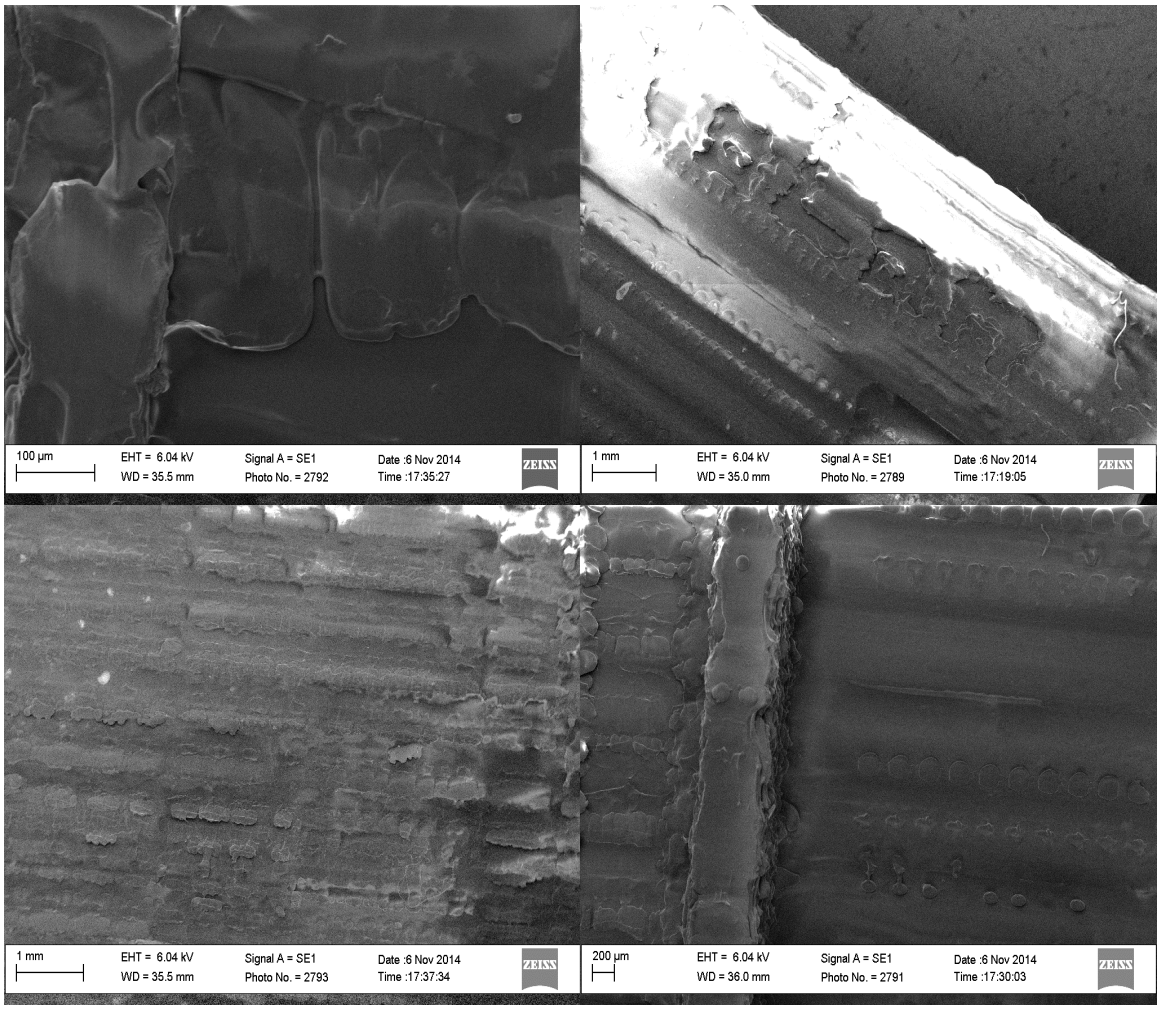

Figure 22: SEM images of the 30μm microridged 3D printed piece

The overall conclusion from these images was that the 3D printer was unable to print the 60μm ridges on the piece. The top left image is shown with the scale of 100μm. At this magnification the ridges should be clearly visible, however the surface appears to be mostly smoothed over. The top right image shows that the printer was able to print "Nolan" into the surface of the piece. However, the bubbly, curvy letters show the imperfection of the printing process. The printer was unable to form the straight lines specified in the design. These horizontally oriented imperfections can also be seen on the separating ridge in the bottom right

image. While the top surface of the ridge is mostly smooth, the walls of the ridge are jagged and rough. This image also shows that while the microridges are not present, the left side of the piece does look rougher than the smooth side on the right. The bottom left image is zoomed out to make clear the horizontal lines formed during the 3D printing process. One potential way to mitigate the effects of these grooves would be to print the piece rotated 90 degrees so that the grooves are oriented in the same direction as the microridges.

The SEM imaging showed that the 3D printer was not able to print 60μm ridges into a flat piece. From viewing the images, it appeared that the printer was able to print with higher resolution vertically rather than horizontally. This was evident when viewing the letters printed at a depth of 100μm as well as the separating ridge in the middle of the piece. Both of these features seemed smooth and accurate on the surfaces, yet rough and construed on the sides. Fabricating more test pieces with varying ridge widths and depths could provide more insight into the problem.

Appendix C: Arduino Code

```
int const powerPin=5;
int const dirPin=4;
int const resetPin=6;
int const FF1Pin=7;
int const FF2Pin=8;
int const ButtonPin=9;

void setup() {
 pinMode(13,OUTPUT); //Pin on board is connected to pin 13.
 digitalWrite(13,LOW);
 pinMode(ButtonPin,INPUT_PULLUP);
 pinMode(dirPin,OUTPUT);
 pinMode(resetPin,OUTPUT);
 pinMode(FF1Pin,INPUT);
 pinMode(FF2Pin,INPUT);
 digitalWrite(dirPin,HIGH);
 digitalWrite(resetPin,LOW);//turns motor driver off

//wait for switch
// while(digitalRead(buttonPin)){
// delay(10);
// }

 digitalWrite(resetPin,HIGH);//turns motor driver on
 delay(100);
}

void loop() {
 checkfaults();
 analogWrite(powerPin,0);
 delay(15000);
 analogWrite(powerPin,220); //Between 0 and 255
 delay(5000); //in ms
 checkfaults();
}

//This function will turn the LED connected to pin 13 on
//if there is a fault
void checkfaults(){
  if(digitalRead(FF1Pin)){
    digitalWrite(13,HIGH);
  }
  if(digitalRead(FF2Pin)){
      digitalWrite(13,HIGH);
  }
}
```